

DMODE: Differential Monocular Object Distance Estimation Module without Class Specific Information

Pedram Agand ^{1*}, Michael Chang ¹, and Mo Chen ¹

¹Department of Computer Science, Simon Fraser University, Burnaby, BC, Canada.

Abstract

Using a single camera to estimate the distances of objects reduces costs compared to stereo-vision and LiDAR. Although monocular distance estimation has been studied in the literature, previous methods mostly rely on knowing an object's class in some way. This can result in deteriorated performance for dataset with multi-class objects and objects with an undefined class. In this paper, we aim to overcome the potential downsides of class-specific approaches, and provide an alternative technique called DMODE that does not require any information relating to its class. Using differential approaches, we combine the changes in an object's size over time together with the camera's motion to estimate the object's distance. Since DMODE is class agnostic method, it is easily adaptable to new environments. Therefore, it is able to maintain performance across different object detectors, and be easily adapted to new object classes. We tested our model across different scenarios of training and testing on the KITTI MOTS dataset's ground-truth bounding box annotations, and bounding box outputs of TrackRCNN and EagerMOT. The instantaneous change of bounding box sizes and camera position are then used to obtain an object's position in 3D without measuring its detection source or class properties. Our results show that we are able to outperform traditional alternatives methods e.g. IPM (Tuohy et al. 2010), SVR (Gökçe et al. 2015), and (Zhu and Fang 2019) in test environments with multi-class object distance detections.

Introduction

For the safety and navigation of autonomous cars and their passengers, the ability to precisely estimate object distances is essential. Additionally, simultaneous localization and mapping (SLAM), virtual reality and surveillance video perception (Zhang et al. 2020b; Agand et al. 2022; Yang et al. 2019; Kang et al. 2019) can all benefit from the usage of distance information. Hence, real-time spatial comprehension, including precise multiple object distance estimates and tackling the existing issues is a major focus in visual distance estimation.

Traditionally, the distances of objects are calculated by either a stereo/multi-camera imaging system or by LiDAR measurements, both of which have disadvantages that impact their use cases and scalability. Stereo-imaging requires

two cameras and precise synchronization between them to produce rectified image pairs (Chen et al. 2020), this can introduce multiple points of failure. A failure of either one of the cameras or the synchronization module would cause the complete loss of functionality. In addition, stereo vision is limited by the distance between the two cameras and the existence of texture in the region of interest (Saxena et al. 2007). By eliminating these extra requirements that are associated with stereo vision also reduces the costs of each system, and therefore increased scalability. While accurate, LiDAR systems are substantially more expensive to buy and operate than a single camera. Although self-contained, a LiDAR device has several moving parts and components that each potentially fail (Reyes Duran et al. 2013). Equipping a vehicle with multiple LiDAR devices for redundancy is incredibly cost prohibitive. Waymo (Sun et al. 2020), an autonomous driving research group, uses LiDAR devices costing around \$7500 USD in 2019 (Moreno 2021). A system that utilizes a single camera could incorporate tens of backup cameras for the price of a single LiDAR device.

Monocular object distance estimate techniques now in use are either inaccurate or labor-intensive in terms of data collecting. Monocular vision has significant difficulties when estimating object distance. Modern monocular object distance estimate systems typically offer three different sorts of solutions. Combining a 2D object detector and a monocular image depth estimator is the first solution. The 2D object detector finds object boxes or masks from the image, and the monocular depth estimator produces depth information for the whole image. The depth information for pixels inside the detected box is then extracted by applying the detected boxes or masks to the depth picture. The system's fundamental flaw is that it mainly relies on a monocular depth estimator, which is not intended for precise object-wise depth estimate. Utilizing a monocular 3D object detector is the second option. These detectors can provide 3D bounding boxes (BBox) for objects, which show how far apart they are. Since they are trained to predict complete 3D box information from object-specific data, including 3D position, size, and rotation, rather than just depth of the entire image, 3D object detectors are often more accurate. Such detectors, however, need additional annotations of 3D BBox coordinates for training, necessitating specialised equipment and high labelling expenses.

*pagand@sfu.ca

There have been studies looking into using deep neural networks to directly estimate object distance in the third solution. One of the earlier object distance estimation methods is inverse perspective mapping (IPM) (Tuohy et al. 2010), which operates by converting points or BBox on the image to its corresponding birds-eye view coordinates. Due to the nature of the approach however, IPM does not work as well for far away objects (about 40m) or where the road is not straight (Zhu and Fang 2019). Another contemporary method utilizes a CNN feature extractor with distance and keypoint regressors (Zhu and Fang 2019). Their method includes results with and without using an object classifier. The authors in (Zhang et al. 2020b) use a modified MaskR-CNN, with the mask head replaced by the depth head; this is then combined with the camera’s extrinsic matrix as input for a shallow GeomNet (Barequet et al. 1999). The authors in Yu and Oh (2021) also estimate object distances using BBoxes. To improve the accuracy compared to rudimentary BBox methods, they use “anchors” to group objects to be processed by specific predictors.

A class specific approach that uses the raw appearance of the object detection can only be accurate when their operational environment matches that of its training. Consider an experiment with a test scenario of toy objects. A toy car at the same distance away as a real car will look much smaller, but may still be detected as a “Car” by object classification networks. Another case is when the object is presented in the camera field of view while it is tilted. A class specific approach can only detect the distance correctly if the object is in the dataset with the exact pose, which is not likely, or requires an enormous dataset. Finally, the precision in the class-specific approaches with multiple classes are limited to the accuracy of the classification technique, however, this is not the case for class-agnostic approaches. For instance, in a class-agnostic approaches, it does not matter whether the object is a car or a pedestrian.

In this paper, we present a differential method to estimate the distances of object without using any information specific to the object’s class. This is done to prevent model from memorizing the typical sizes of different types of objects at certain distances away. Instead, our method will utilize the object’s change of projected size over time in combination with the camera’s motion to estimate its distance. The main properties of our approach (DMODE) are as follows: 1) ability to provide accurate distance estimations without using any explicit or implicit information relating to the object’s class 2) independency from camera intrinsic parameter 3) *generalizability*, which enables reasonably accurate distance estimation on unseen classes of objects, followed by ability to transfer learning for new classes 4) *adaptability*, that is applicable to different object tracking network (OTN) 5) *train once, use everywhere* property, in which the model is able to maintain accuracy when the source of object detection is different from what it was trained with. The code is available at <https://github.com/anonym-paper/DMODE>.

Related work

In this section, we review different methods for monocular distance estimation. We chose object depth estimation

prospective to address the problem of multi-class distance estimation without class-specific information.

Monocular depth estimation

In order to do depth estimation over an entire image, a deep neural network using continuous condition random fields for image patches was proposed by Liu et al. (2015). The accuracy of depth estimation was improved by Fu et al. (2018) who added ordinal regression to the depth estimation network and used scale-increasing discretization to convert continuous depth data to an ordinal class vector. These techniques require extremely heavy costs of manpower and computing resources with specific training images data and corresponding depth map of each pixel (Zhang et al. 2020a). In the absence of a depth image serving as the ground-truth, unsupervised training might make use of additional depth cues from stereo images (Godard, Mac Aodha, and Brostow 2017) or optical flows (Godard et al. 2019). A novel deep visual-inertial odometry and depth estimation framework is presented by Wan et al. (2022) to increase the precision of depth estimation and ego-motion using picture sequences and inertial measurement unit (IMU) raw data. Unsupervised depth estimation methods, have inherent scale ambiguity and poor performance due to the lack of perfect ground-truth and geometric constraints (Wan et al. 2022).

Monocular 3D object detection

The difficult job of 3D object recognition from monocular pictures is connected to object distance estimate. Mousavian et al. (2017) presented the Deep3DBox, which uses a 3D regressor module to estimate the 3D box’s dimensions and orientation and accepts 2D detection input to crop the input characteristics. To replace the widely used 2D R-CNN structure, Brazil and Liu (2019) presented a 3D region proposal network, which greatly improved performance. Additionally, some studies use point cloud detection networks or monocular depth estimation networks as supplementary components of monocular 3D object identification (You et al. 2019). These additional details increased the 3D object detection networks’ accuracy.

Monocular object distance estimation

Utilizing camera characteristics and vehicle height as inputs, Ali and Hussein (2016) used a geometric model to determine how far apart two cars were from one another. If any vehicle with a different height comes, this strategy would fail. A lightweight network was employed by Bertoni, Kreiss, and Alahi (2019) to predict human position from 2D human postures. By adding a depth regression module to the Faster R-CNN based structure and an additional keypoint regressor to enhance performance for objects close to the camera, Zhu and Fang (2019) made a significant contribution to the field of generic object distance estimation. A framework that splits the problem of monocular 3D object identification into a few smaller tasks, including object depth estimation, was suggested by Cai et al. (2020). In order to address the information loss caused by the 3D to -2D projection, they suggested a height-guided depth estimation technique. A network with an R-CNN based structure was used by Zhang

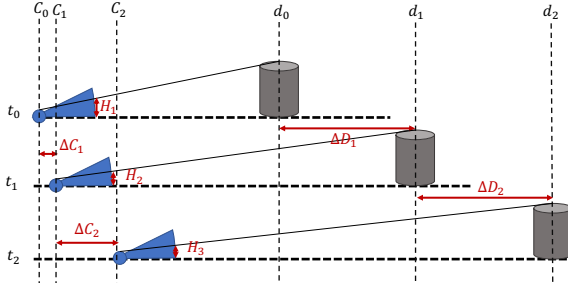


Figure 1: Variables in DMODE: a mathematical view point

et al. (2021) to achieve object identification and distance estimate concurrently.

Problem statement

Our objective in this paper is to estimate the distances of objects by calculating their relative Cartesian position to a single camera without using any information relating to its class. The camera may be mounted on a moving vehicle, or stationary. In both cases, we will combine measurements of an inertial measurement unit (IMU) with the outputs of an OTN as input for our model. We assume the following: 1) The distance between object and the camera in the captured frames are different. This change can be caused by movement of the object, camera or both. 2) Camera movement (velocity) is measured by an IMU. 3) The object does not have any angular velocity in yaw direction within the captured frames. (Yaw direction is orthogonal to roll direction -car turning left/right- and pitch direction -tilting around axis connecting the camera and the object). Note that if the object is tilted in yaw direction and remain the same angle for the following frames, the framework can still function successfully.

For the sake of illustration, Fig. 1 depicts a 1D scenario with three time instants, t_0, t_1, t_2 . Let d_j be the object's distance from the camera, D_j be the object's absolute position, H_j the object's size as captured by the camera, and C_j the camera's absolute position at time t_j . In addition, define $\Delta F_j = F_j - F_{j-1}$, where F can be any of the aforementioned variables. For convenience, suppose $\Delta t = t_2 - t_1 = t_1 - t_0$ and $C_0 = 0$. Our objective is to compute d_2 , the object's relative position with respect to the camera at the current (latest) time, given $H_0, H_1, H_2, \Delta C_1, \Delta C_2$. In the 3D case, we would like to determine a function that outputs the relative coordinates of the object $\phi = (x, y, z)$ with respect to the camera.

$$\phi = \mathcal{F}(H_1, H_2, \dots, H_{q+1}, \Delta C_1, \Delta C_2, \dots, \Delta C_q), \quad (1)$$

where $q + 1$ is the number of input frames and \mathcal{F} is an unknown function we would like to determine. To alleviate the effects of noisy measurements and potential errors in object tracking in practice, we will add other inputs to the function \mathcal{F} and utilize a deep neural network. Then the distance to the center of the object is calculated using the following relation:

$$d = \sqrt{x^2 + y^2 + z^2} \quad (2)$$

Method

Our method involves tracking the projected size of an object in the camera lens over a predefined time frame while taking into account the camera's motion to estimate the object's distance from the camera. To achieve this, we require an OTN and an Inertial Measurement Unit (IMU) for the camera. To prove feasibility of our approach, we use mathematical derivation to obtain this distance assuming perfect measurement. Later, we will utilize a deep neural network to handle uncertainty and nonlinearity for real-world applications (Agand, Motaharifar, and Taghirad 2017).

Analytic solution

For the sake of illustration, we derive the relative distance for the simplified 1D scenario illustrated in Fig. 1. We will be using the difference in the projected image of the object in camera lens using the following relation:

Axiom: Object size and distance is inversely proportional (Alphonse and Sriharsha 2021)

$$\frac{d_{n-1}}{d_n} = \frac{H_n}{H_{n-1}} \doteq P_n \quad (3)$$

Theorem: Given $q + 1$ frames, the following relations apply for all $i \in \{1, 2, \dots, q\}$:

$$(1 - p_i) \sum_{k=i+1}^{q+1} \Delta D_k + \Delta D_i = \sum_{k=i}^q \Delta C_k - p_i \sum_{k=i+1}^q \Delta C_k \quad (4)$$

where $d_j = \Delta C_j = 0, \forall j > q$.

Proof. According to Fig. 1, we have:

$$d_n = d_{n-1} + \Delta D_n - \Delta C_n \quad (5)$$

First let us prove the last relation ($i = q$) in (4). By using Eq. (3) for $n = q$, we have $d_{q-1} = p_q d_q$, which can be substituted in (5) for $n = q$. This proves the last relation in (4) ($i = q$), since $\Delta D_{q+1} = d_q$, we have:

$$p_q = \frac{d_q - \Delta D_q + \Delta C_q}{d_q} \quad (6)$$

Now for $i = q - 1$, we can write similar relation to (6) as follows by considering the previous time step and substituting d_{q-1}, d_{q-2} using (3) for $n = q, q - 1$:

$$d_q p_q = p_{q-1} d_{q-1} + \Delta D_{q-1} - \Delta C_{q-1} \quad (7)$$

Using the relation for p_q in (6), we can simplify the relation in (7) as follows:

$$(d_q - \Delta D_q + \Delta C_q)(1 - p_{q-1}) = \Delta D_{q-1} - \Delta C_{q-1} \quad (8)$$

which is equivalent to the second last relation in (4) ($i = q - 1$). The proof for other relations follows the same pattern. Now we need to integrate the assumption about object movement into ΔD_j variables to reduce one of them as unknown variable (i.e for object with constant velocity we have $\Delta D = V\Delta t$ or with constant acceleration, $\Delta D = 1/2a\Delta t^2 + V\Delta t$). The general relation is as follows:

$$\underline{\mathbf{A}}(P)[d_q, \underline{\mathbf{f}}]^T = \underline{\mathbf{b}}(C, P) \quad (9)$$

where \underline{A} is a $q \times q$ matrix of (P_1, \dots, P_q) parameters, \underline{f} is a row vector of relative movement components (e.g. velocity, acceleration, etc), and \underline{b} is a column vector of $(P_1, C_1, \dots, P_q, C_q)$ parameters. The analytic solution to derive distance in Eq. (9) is given by:

$$d_q = \underline{A}_1^{-1} \underline{b}(C, P) \quad (10)$$

where A_1^{-1} is the first row of A inverse. \square

For the special case, where the objects of interest is stationary, $q = 1$ and the relation will be simplified to:

$$(1 - p_1)d_1 = \Delta C_1, \text{ if } q = 1 \quad (11)$$

In this paper we assume objects moving with constant velocity which requires $q = 2$. Hence, $\Delta D_1 = \Delta D_2 = \Delta D$ and Eq. (9) will be:

$$\begin{bmatrix} P_1 - 1 & 2 - P_1 \\ P_2 - 1 & 1 \end{bmatrix} \begin{bmatrix} d_2 \\ \Delta D \end{bmatrix} = \begin{bmatrix} \Delta C_1 + \Delta C_2 - P_1 \Delta C_2 \\ \Delta C_2 \end{bmatrix} \quad (12)$$

Where we can solve for d_2 and ΔD .

$$d_2 = \frac{\Delta C_1 - \Delta C_2}{P_1 P_2 - 2P_2 + 1}, \text{ if } q = 2 \quad (13)$$

This means that analytically, if the object is moving with constant velocity, the camera should not be moved with a constant velocity. However, as mentioned before, upon inspection of the ground-truth annotations, the change of an object's BBox size is often inconsistent with its distance changes from the camera. With this in mind, we utilize a neural network and try to fit it to these and other discrepancies in the dataset.

Network architecture

Our network is a sequential network comprised of a 2D convolution neural network (CNN), and a 1D multi-layer perceptron (MLP) with soft-plus activation and normalization between each layer. We are using ResNet-18 ($\mathcal{F}_{ResNet18}$) from (He et al. 2016) as the 2D net, then concatenating selected IMU and BBox information onto its output before feeding it through the 1D net (\mathcal{F}_{MLP}).

After processing detected object from OTN (\mathcal{F}_{OTN}), it will fed through ResNet-18 which result 1000 parameter as latent variables (\mathcal{Z}). This output is then concatenated with an extra 34 parameters, 27 of which consists of the camera's cartesian velocities, accelerations, and angular accelerations of the 3 keyframes (\mathcal{X}), 6 parameters are the object's BBox centres in relation to image dimensions (C_B), which is the only bounding information that are not related to its class. The last parameter is the analytic solution to the problem (d_2) given by Eq. (13).

$$\begin{aligned} I_{B,t_i} &= \mathcal{F}_{OTN}(I_{t_i}); \quad \forall i \in \{0, 1, 2\}, \\ I_{B,t_i}^* &= \mathcal{F}_{map}(I_{B,t_0}, I_{B,t_1}, I_{B,t_2}); \quad \forall i \in \{0, 1, 2\}, \\ \mathcal{Z}_{(1 \times 1000)} &= \mathcal{F}_{ResNet18}(I_{B,t_0}^*, I_{B,t_1}^*, I_{B,t_2}^*), \\ [x, y, z] &= \mathcal{F}_{MLP}(\mathcal{Z}, C_{(1 \times 6)B}, \mathcal{X}_{(1 \times 27)}, d_2), \end{aligned} \quad (14)$$

where, $I_{t_i}, I_{B,t_i}, I_{B,t_i}^*$ are the image frame, the BBox image (object's RGB data and the BBox information), and the processed BBox image in time frame t_i , respectively. Note that \mathcal{F}_{map} is the processing stage function that will be noted in the learning framework section. This 1034 long tensor is fed through an MLP to obtain the three separate parameters [x, y, z], Cartesian positions. Separated output into ortho-basis vectors at training the model is compared to a singular distance value by using Eq. (2).

Learning framework

The framework of the system is shown in Fig. 2. Each detected object at any frame invokes a check of the cached data. If there exist detection data of this object for all the keyframes, it will get prepared for distance estimation by \mathcal{F}_{map} in the following stage: The detected objects are cropped out along their BBox and converted to single channel greyscale images. For each object, the system will collects its images frame and BBox information (I_{B,t_i}) of the keyframes corresponding to t_0, t_1 , and t_2 . The triple of images is then resized relatively according to the heights of their BBoxes while retaining their original aspect ratios, with the largest of the three scaled to 224px in height. The 3 images are padded/cropped to the size of 224×224 , then centre-overlaid on top of each other in the order of detections at t_0, t_1 , then t_2 . This newly formed 3 channel image is the 2D input to ResNet-18.

Note that \mathcal{F}_{OTN} in Eq. (14) is a pre-trained network, \mathcal{F}_{map} is an arithmetic manipulation, and only $\mathcal{F}_{ResNet18}, \mathcal{F}_{MLP}$ networks are trained simultaneously. The objective function is based on robust Adaptive Reverse Huber Loss (BerHu) (Lambert-Lacroix and Zwald 2016):

$$B(\phi, \phi^*) = \begin{cases} |\phi - \phi^*|, & \text{if } |\phi - \phi^*| \leq c, \\ \frac{(\phi - \phi^*)^2 + c^2}{2c}, & \text{otherwise} \end{cases} \quad (15)$$

where ϕ^* is the corresponding ground-truth of Cartesian space, and $c = 0.2 \cdot \max(|\phi - \phi^*|)$. Both L1 and L2 features are present in the BerHu loss, which responds adaptively to the c value. In contrast to the L2 loss function, the BerHu loss function converges more quickly while effectively maintaining small residuals because it is differentiable at the point c when the switching between L1 and L2 losses takes place. This will help the network to utilize the shrinkage power of L1 norm to avoid low gradients for relatively small residuals. The data loss is defined as follow:

$$L = \frac{1}{3N} \sum_{i=1}^N (B(x_i, x_i^*) + B(y_i, y_i^*) + B(z_i, z_i^*)) \quad (16)$$

where N is the number of mini-batch samples, and i denotes the object index of all the images belonging to the current batch. We used the ADAM optimizer with a weight decay of 1e-5 (Agand and Shoorehdeli 2019). To avoid gradient vanishing for the deep networks, we use dropout and batch normalization technique (Garbin, Zhu, and Marques 2020).

Results

To measure the various properties of our method, we present its performance in the following scenarios. Ground-Truth

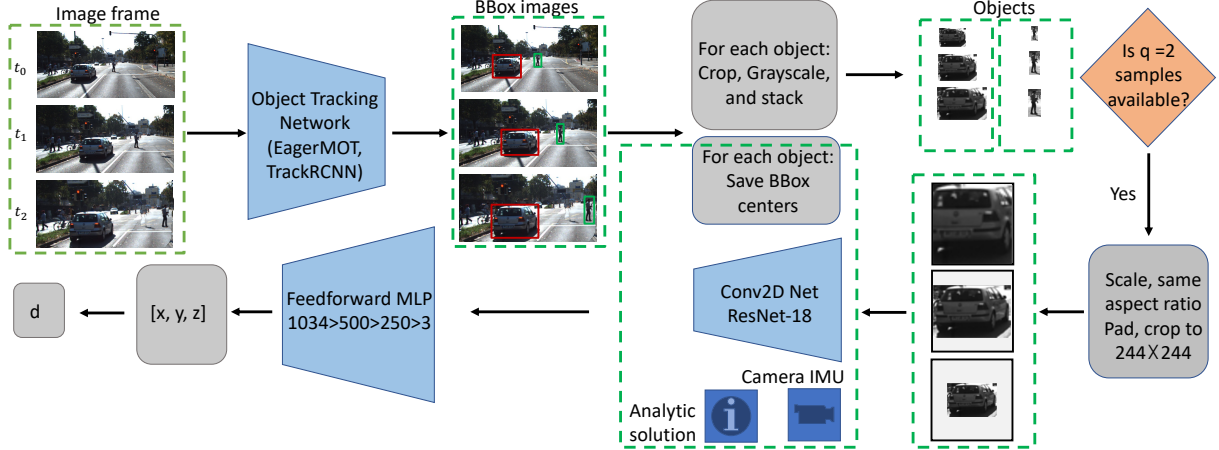


Figure 2: DMODE framework: workflow of data and models

has been abbreviated to GT, TrackRCNN to TRCNN, and EagerMOT to EMOT.

Model setup

Our model estimates distances based off of the evolution in an object’s size overtime in conjunction with the camera’s movements. To fit with ResNet-18’s input parameters, we will be using a 3-interval scheme that mathematically assumes a constant velocity. In order to measure a perceivable difference, we have chosen 1 second as the look-back time frame. Since KITTI’s camera records in 10fps, the keyframes for this scheme will be frames n, n-5, and n-10 corresponding to t_2 , t_1 , and t_0 respectively.

For our dataset, we are using the KITTI Multi Object Tracking’s (Milan et al. 2016) images, annotations, and IMU data. This dataset includes detection, classification, and tracking data for 7 classes: “Car”, “Van”, “Truck”, “Pedestrian”, “Person Sitting”, “Cyclist”, and “Tram”. Most of the scenes was recorded with a car driving through urban and residential areas, with a few recorded by a stationary camera. From the KITTI dataset, we are excluding object detections that have been labeled as class “Misc” or “DontCare”. Due to the nature of our approach, we have also filtered out all entries where the object is not fully in frame. This is accompanied by the mechanism to discard any object detections with BBoxes touching the edge of the frame during testing. Finally, occluded object detections are excluded from training in order to maintain consistency among the images.

We define the size of objects by the height of its BBox. In a non-synthetic environment, it is far more likely for an object to yaw left and right (i.e., a car turning), and thereby increasing its horizontal size, than to pitch up and down. This makes the height of an object to be the most consistent indicator of its change in distance from the camera. Our training and validation split is in accordance with KITTI’s data separation, used by TrackRCNN and EagerMOT. Our results are obtained from the validation set. Each model is trained over 100 epochs, with a batch size of 32 and learning rate of 1e-3. Training data was randomly ordered between each epoch. We are estimating the distances to the centres of objects, as

defined by KITTI’s 3D BBox annotations, not the closest point to the camera.

Object tracking network (OTN) To demonstrate that our method can maintain its performance when using data generated by other sources, we will be using the outputs of TrackRCNN (Voigtlaender et al. 2019) and (Kim, Osep, and Leal-Taixé 2021) as object tracking inputs for comparison. A limitation of these networks is that while KITTI annotations contain detections for 7 classes of objects, TrackRCNN and EagerMOT only detects cars and pedestrians.

Data alignment The object ID outputs of the OTN do not always match the ID assigned by ground-truth annotations. This is because object tracking only requires each object to be assigned some unique identifier to differentiate from other objects throughout the scene. In order to assign ground-truth distances to each detected object at each frame, the BBox outputs of the OTN are compared against the ground-truth BBoxes. The ground-truth annotation of some object is assigned to one of the tracking network’s outputs if it maximizes the formula out of all the detections:

$$BOX_{pred} \cap BOX_{GT} - BOX_{pred} \oplus BOX_{GT} \quad (17)$$

Evaluations For evaluation of our method with different methods we use the following common metric. Each metric has a corresponding mark where \downarrow means “lower is better” and \uparrow means “higher is better”.

Mean absolute relative error (MARE \downarrow):

$$MARE = \frac{1}{N} \sum \left(\frac{\|d_i^* - d_i\|}{d_i} \right) \quad (18)$$

Median relative error (MRE \downarrow):

$$MRE = Median(\|d_1^* - d_1\|, \dots, \|d_n^* - d_n\|) \quad (19)$$

95% confidence interval (.95CI \downarrow):

$$Rel. Err. \pm x = .95CI \quad (20)$$

Root mean square error (RMSE \downarrow):

$$RMSE = \sqrt{\frac{1}{N} \sum \|d_i^* - d_i\|^2} \quad (21)$$

Threshold ($\delta \uparrow$):

$$\delta = \text{Max}(d_i/d_i^*, d_i^*/d_i) \% < 1.25 \quad (22)$$

Square relative difference (SRD \downarrow):

$$SRD = \frac{1}{N} \sum \left(\frac{\|d_i^* - d_i\|^2}{d_i} \right) \quad (23)$$

$\text{RMSE}_{\log} \downarrow$:

$$RMSE_{\log} = \sqrt{\frac{1}{N} \sum \|\log d_i^* - \log d_i\|^2} \quad (24)$$

Baseline and dataset robustness testing

As a baseline, the model's performance tested on the full annotation of the validation set is showed in Table 1. To test if our method is robust in regard the dataset, our model's performance when fed different sources of detections of the validation set. The model was trained on the full annotations of the ground-truth training set. Because EagerMOT and TrackRCNN only detects "Cars" and "Pedestrians", we also include the class limited ground-truth results as a baseline (G^*). In comparison, our model's performance when it was trained and tested on TrackRCNN's outputs is shown in the last row of Table 1.

Table 1: Models trained and tested on GT or OTN

Train type	Test type	MARE \downarrow	MRE \downarrow	.95CI \downarrow	RMSE \downarrow
GT	GT	0.145	0.107	3.9e-3	6.765
GT	GT*	0.138	0.107	3.2e-3	6.676
GT	TRCNN	0.168	0.125	4.6e-3	7.139
GT	E-MOT	0.160	0.124	3.7e-3	6.435
TRCNN	TRCNN	0.163	0.118	4.8e-3	7.202

Class agnostic testing

The measure of how our method performs against a class of object that was excluded from training is shown in Table 2. In addition, we also examine the increase in accuracy with transfer learning (TL) training of the missing class.

Table 2: Model tested only cars class on GT

Training classes	MARE \downarrow	MRE \downarrow	.95CI \downarrow	RMSE \downarrow
All	0.143	0.113	4.1e-3	7.821
No Car	0.282	0.243	6.6e-3	13.923
TL	0.173	0.133	4.9e-3	9.356

Comparison

We compare our method against other object distance estimation methods in table 3. We used EagerMOT as the OTN with the model trained on the full set of ground-truth annotations for all evaluation scenarios. Accuracy measurements for IPM (Tuohy et al. 2010) and SVR (Gökçe et al. 2015) were sourced from Zhu and Fang (2019)'s experiments. In singular-class evaluations (car only and pedestrian only), our model performed worse compared to (Yu and Oh 2021) and (Zhang et al. 2020b). In comparison to (Zhang et al. 2020b), our model performed better in MARE and RMSE_{\log} while worse in Sqr Rel and RMSE. This indicates that while our model is more accurate on average, there are more extreme outliers. For the multi class training, which was the main goal of this research, against the few methods that provided results in multi-class testing, our model was able to outperform them in every metric. We were not only able to surpass the performance of Zhu and Fang (2019)'s non-class-specific version of their model, but also the version using a classifier. For the Zhang MaskRCNN method, the result for average was not reported. Yet, the valid rate (VR) was mentioned which captures ratio of successfully detected objects number to total objects number. This value for their approach is 0.822 meaning that for around 20% of the objects, the object can not identify the distance correctly, as it will be a misrepresentation in the data. Yet, this problem is not an issue in our approach, as the learned knowledge is transferable to the new class. In addition, Yu log-scale anchors method does not provide any result or discussion for multi class or pedestrian distance estimation.

Discussion

Experiment result analysis

The dataset agnostic testing demonstrated that our method can be trained once on ground-truth annotations then fed outputs of different object tracking outputs without a significant loss in accuracy. Furthermore, specifically training on the outputs of the OTN used for testing yielded similar accuracy than if the model was trained on ground-truth annotations. This shows that our model can be deployed across multiple different systems, each with their own OTN, without requiring retraining while maintaining its accuracy. Class agnostic testing showed that the model's accuracy dropped significantly when estimating the distances of a class of object it has never seen before.

Error analysis

The model for this analysis was trained on ground-truth then tested on the validation set with EagerMOT object tracking and detection. Based on the results in Fig. 3, our method performed well for objects at distances between 5 to 60 metres, where most of the object detections are functional. The reason for a pick in relative error for objects within 5 meters are due to the lack of training population. The lack of samples less than 5 meters away is because we have excluded object detections that have been truncated by the camera's field of view. The rapid increase in errors for ranges above 60 metres is due to the lack of resolution in the camera and/or 2D input

Class type	Method	$\delta < 1.25 \uparrow$	MARE \downarrow	Sqr Rel \downarrow	RMSE \downarrow	RMSE _{log} \downarrow
Car only	SVR	0.345	1.494	47.748	18.970	1.494
	IPM	0.701	0.497	35.924	15.415	0.451
	Enhanced vgg16	0.848	0.161	0.619	3.580	0.228
	MaskRCNN	0.992	0.049	-	1.931	-
	log-scale anchors	0.972	0.073	0.150	1.195	0.117
	Ours	0.773	0.159	1.467	7.241	0.223
Pedestrian only	SVR	0.129	1.499	34.561	21.677	1.260
	IPM	0.688	0.340	543.223	192.177	0.348
	Enhanced vgg16	0.747	0.183	0.654	3.439	0.221
	MaskRCNN	0.991	0.049	-	2.043	-
	Ours	0.767	0.162	0.932	4.567	0.192
Average on Multiple classes	SVR	0.379	1.472	90.143	24.249	1.472
	IPM	0.603	0.390	274.785	78.870	0.403
	Enhanced vgg16	0.486	0.541	5.555	8.747	0.512
	Enhanced vgg16	0.629	0.251	1.844	6.870	0.314
	Ours	0.771	0.160	1.280	6.435	0.213

Table 3: Comparing between SVR (Gökçe et al. 2015), IPM (Tuohy et al. 2010), enhanced vgg16 (Zhu and Fang 2019), MaskRCNN (Zhang et al. 2020b), log-scale anchors (Yu and Oh 2021), ours (GT train; EagerMOT test)

to represent the differences in the object’s change in size (i.e. 70/65 is smaller than 60/55 despite having the same change in distance).

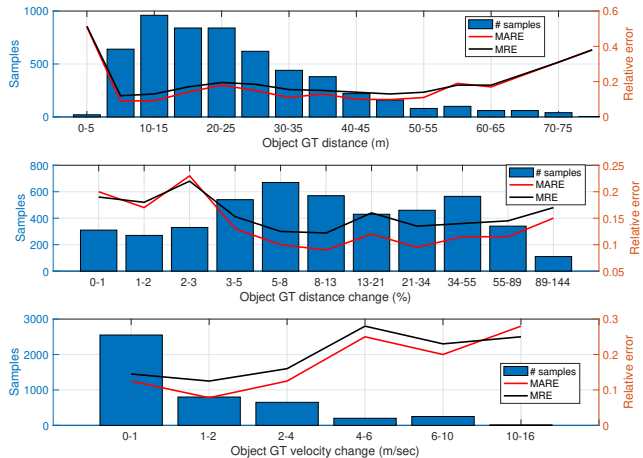


Figure 3: Error bar in relation to distance, distance change and velocity change. The red line represents MARE and the black line represents the MRE and the bars shows the number of samples in each bin

Our analysis on the second subplot in Fig. 3 shows that the model performed better on objects that have significantly changed its relative distance from the camera over the interval than those that have not. A 3-5% difference between the first and last interval was enough to produce significant improvements to the model’s accuracy. As earlier mentioned in our mathematical motivation section, the 3-interval version of the method is only suitable to objects with constant velocity. This analysis on the third subplot shows that our model has good accuracy for objects with less than 2m/s change

in velocity, but quickly deteriorates for objects with larger changes in its motion. On another note, most objects did not change their velocity more than 2m/s. For use cases such as driving through a city as recorded in the KITTI dataset, our current model is able to provide distance estimations within 13.5% relative error on average despite its limitations.

Conclusion

A method of estimating object distances without any class specific information by using the evolution of the object’s appearance overtime in conjunction with the camera’s motion was presented. Thanks to our inherent approach property, class agnosticity, the model can transfer knowledge by supplemented training with samples of the targeted class. In addition, our approach provide acceptable outcome for the multi-class distance estimation, despite its competitor in the literature. Although DMODE accuracy depends on the accuracy of the OTN and the key frame selection, the dataset robustness property of our model opens the possibility of a “train once, deploy anywhere” scheme of operation. The most significant drawback of our approach is the time delay before distance estimation is possible. In addition, the object would have to be tracked accurately over three key frames that matches the time intervals used during training. According to the network architecture described in this paper, it only had 3 channels for their input parameters which only allowed us to implement the most basic version of our approach which assumed the object to have constant velocity. Although the results are satisfactory, there are many outliers in the error profile that we are assuming to be objects that are changing their motions very quickly. Increasing the channel capacity of our 2D network to accommodate for more intervals to increase the model’s performance on these objects can be considered as future direction.

References

Agand, P.; Motaharifar, M.; and Taghirad, H. D. 2017. Tele-operation with uncertain environment and communication channel: An H_∞ robust approach. In *2017 Iranian Conference on Electrical Engineering (ICEE)*, 685–690. IEEE.

Agand, P.; and Shoorehdeli, M. A. 2019. Adaptive model learning of neural networks with UUB stability for robot dynamic estimation. In *2019 International Joint Conference on Neural Networks (IJCNN)*, 1–6. IEEE.

Agand, P.; Taherahmadi, M.; Lim, A.; and Chen, M. 2022. Human Navigational Intent Inference with Probabilistic and Optimal Approaches. In *2022 International Conference on Robotics and Automation (ICRA)*, 8562–8568. IEEE.

Ali, A. A.; and Hussein, H. A. 2016. Distance estimation and vehicle position detection based on monocular camera. In *2016 Al-Sadeq International Conference on Multidisciplinary in IT and Communication Science and Applications (AIC-MITCSA)*, 1–4. IEEE.

Alphonse, P.; and Sriharsha, K. 2021. Depth perception in single rgb camera system using lens aperture and object size: a geometrical approach for depth estimation. *SN Applied Sciences*, 3(6): 1–16.

Barequet, G.; Duncan, C. A.; Goodrich, M. T.; Bridgeman, S. S.; and Tamassia, R. 1999. GeomNet: Geometric computing over the Internet. *IEEE Internet Computing*, 3(2): 21–29.

Bertoni, L.; Kreiss, S.; and Alahi, A. 2019. Monoloco: Monocular 3d pedestrian localization and uncertainty estimation. In *Proceedings of the IEEE/CVF International Conference on Computer Vision*, 6861–6871.

Brazil, G.; and Liu, X. 2019. M3d-rpn: Monocular 3d region proposal network for object detection. In *Proceedings of the IEEE/CVF International Conference on Computer Vision*, 9287–9296.

Cai, Y.; Li, B.; Jiao, Z.; Li, H.; Zeng, X.; and Wang, X. 2020. Monocular 3d object detection with decoupled structured polygon estimation and height-guided depth estimation. In *Proceedings of the AAAI Conference on Artificial Intelligence*, volume 34, 10478–10485.

Chen, X.; Wu, X.; Gao, S.; Xie, X.; and Huang, Y. 2020. Synchronization and calibration of a stereo vision system. In *Global Oceans 2020: Singapore – U.S. Gulf Coast*, 1–6.

Fu, H.; Gong, M.; Wang, C.; Batmanghelich, K.; and Tao, D. 2018. Deep ordinal regression network for monocular depth estimation. In *Proceedings of the IEEE conference on computer vision and pattern recognition*, 2002–2011.

Garbin, C.; Zhu, X.; and Marques, O. 2020. Dropout vs. batch normalization: an empirical study of their impact to deep learning. *Multimedia Tools and Applications*, 79(19): 12777–12815.

Godard, C.; Mac Aodha, O.; and Brostow, G. J. 2017. Unsupervised monocular depth estimation with left-right consistency. In *Proceedings of the IEEE conference on computer vision and pattern recognition*, 270–279.

Godard, C.; Mac Aodha, O.; Firman, M.; and Brostow, G. J. 2019. Digging into self-supervised monocular depth estimation. In *Proceedings of the IEEE/CVF International Conference on Computer Vision*, 3828–3838.

Gökçe, F.; Üçoluk, G.; Şahin, E.; and Kalkan, S. 2015. Vision-Based Detection and Distance Estimation of Micro Unmanned Aerial Vehicles. *Sensors*, 15(9): 23805–23846.

He, K.; Zhang, X.; Ren, S.; and Sun, J. 2016. Deep residual learning for image recognition. In *Proceedings of the IEEE conference on computer vision and pattern recognition*, 770–778.

Kang, R.; Shi, J.; Li, X.; Liu, Y.; and Liu, X. 2019. DF-SLAM: A deep-learning enhanced visual SLAM system based on deep local features. *arXiv preprint arXiv:1901.07223*.

Kim, A.; Ošep, A.; and Leal-Taixé, L. 2021. EagerMOT: 3D Multi-Object Tracking via Sensor Fusion. *arXiv preprint arXiv:2104.14682*.

Lambert-Lacroix, S.; and Zwald, L. 2016. The adaptive BerHu penalty in robust regression. *Journal of Nonparametric Statistics*, 28(3): 487–514.

Liu, F.; Shen, C.; Lin, G.; and Reid, I. 2015. Learning depth from single monocular images using deep convolutional neural fields. *IEEE transactions on pattern analysis and machine intelligence*, 38(10): 2024–2039.

Milan, A.; Leal-Taixé, L.; Reid, I.; Roth, S.; and Schindler, K. 2016. MOT16: A benchmark for multi-object tracking. *arXiv preprint arXiv:1603.00831*.

Moreno, J. 2021. Waymo CEO Says Tesla Is Not A Competitor, Gives Estimated Cost Of Autonomous Vehicles.

Mousavian, A.; Anguelov, D.; Flynn, J.; and Kosecka, J. 2017. 3d bounding box estimation using deep learning and geometry. In *Proceedings of the IEEE conference on Computer Vision and Pattern Recognition*, 7074–7082.

Reyes Duran, D.; Robinson, E.; Kornecki, A. J.; and Zalewski, J. 2013. Safety analysis of Autonomous Ground Vehicle optical systems: Bayesian belief networks approach. In *2013 Federated Conference on Computer Science and Information Systems*, 1419–1425.

Saxena, A.; Schulte, J.; Ng, A. Y.; et al. 2007. Depth Estimation Using Monocular and Stereo Cues. In *IJCAI*, volume 7, 2197–2203.

Sun, P.; Kretzschmar, H.; Dotiwalla, X.; Chouard, A.; Patnaik, V.; Tsui, P.; Guo, J.; Zhou, Y.; Chai, Y.; Caine, B.; et al. 2020. Scalability in perception for autonomous driving: Waymo open dataset. In *Proceedings of the IEEE/CVF Conference on Computer Vision and Pattern Recognition*, 2446–2454.

Tuohy, S.; O'Cualain, D.; Jones, E.; and Glavin, M. 2010. Distance determination for an automobile environment using Inverse Perspective Mapping in OpenCV. In *IET Irish Signals and Systems Conference (ISSC 2010)*, 100–105.

Voigtlaender, P.; Krause, M.; Osep, A.; Luiten, J.; Sekar, B. B. G.; Geiger, A.; and Leibe, B. 2019. Mots: Multi-object tracking and segmentation. In *Proceedings of the IEEE/CVF Conference on Computer Vision and Pattern Recognition*, 7942–7951.

Wan, Y.; Zhao, Q.; Guo, C.; Xu, C.; and Fang, L. 2022. Multi-Sensor Fusion Self-Supervised Deep Odometry and Depth Estimation. *Remote Sensing*, 14(5): 1228.

Yang, X.; Luo, H.; Wu, Y.; Gao, Y.; Liao, C.; and Cheng, K.-T. 2019. Reactive obstacle avoidance of monocular quadrotors with online adapted depth prediction network. *Neurocomputing*, 325: 142–158.

You, Y.; Wang, Y.; Chao, W.-L.; Garg, D.; Pleiss, G.; Hariharan, B.; Campbell, M.; and Weinberger, K. Q. 2019. Pseudo-lidar++: Accurate depth for 3d object detection in autonomous driving. *arXiv preprint arXiv:1906.06310*.

Yu, H.; and Oh, J. 2021. Anchor Distance for 3D Multi-Object Distance Estimation from 2D Single Shot. *IEEE Robotics and Automation Letters*, 6(2): 3405–3412.

Zhang, J.; Su, Q.; Wang, C.; and Gu, H. 2020a. Monocular 3D vehicle detection with multi-instance depth and geometry reasoning for autonomous driving. *Neurocomputing*, 403: 182–192.

Zhang, Y.; Ding, L.; Li, Y.; Lin, W.; Zhao, M.; Yu, X.; and Zhan, Y. 2021. A regional distance regression network for monocular object distance estimation. *Journal of Visual Communication and Image Representation*, 79: 103224.

Zhang, Y.; Li, Y.; Zhao, M.; and Yu, X. 2020b. A regional regression network for monocular object distance estimation. In *2020 IEEE International Conference on Multimedia & Expo Workshops (ICMEW)*, 1–6. IEEE.

Zhu, J.; and Fang, Y. 2019. Learning object-specific distance from a monocular image. In *Proceedings of the IEEE/CVF International Conference on Computer Vision*, 3839–3848.